HgTe Quantum Dot based Phototransistor Enabling High Sensitivity Room Temperature Photodetection Beyond 2000 nm Spectral Range

Mengyu Chen[1†], *Haipeng Lu*[1†], *Nema Abdelazim*[2†], *Ye Zhu*[3], *Zhen Wang*[4], *Wei Ren*[4], *Stephen V. Kershaw*[2]*, *Andrey L. Rogach*[2], and *Ni Zhao*[1]*

[1]Department of Electronic Engineering, The Chinese University of Hong Kong, Shatin, New Territories, Hong Kong

[2]Department of Physics and Materials Science and Centre for Functional Photonics (CFP) City University of Hong Kong, Hong Kong S.A.R.

[3]Department of Applied Physics, The Hong Kong Polytechnic University, Hong Kong S. A. R.

[4]Department of Mechanical and Automation Engineering, The Chinese University of Hong Kong, Shatin, New Territories, Hong Kong

† these authors contributed equally to this work.

ABSTRACT

Near-to-Mid infrared photodetection technologies could be widely deployed to advance the infrastructures of surveillance, environmental monitoring and manufacturing, if the detection devices can be made cheaply, in compact format and with high performance. For such

application requirements, colloidal quantum dot (QD) based photodetectors stand out as particularly promising due to the solution processability and integratability with silicon technologies; unfortunately, the detectivity of the QD photodetectors towards longer wavelengths has always been low. Here, we overcome the performance bottleneck through synergistic efforts between synthetic chemistry and device engineering. Firstly, we developed a fully automated aprotic solvent, gas-injection synthesis method that allows scalable fabrication of large sized HgTe QDs with high quality, exhibiting a record high photoluminescence quantum yield of 17% at the photoluminescence peak close to 2.1 μm. Secondly, through gating a phototransistor structure we demonstrate the device response to reach > 2×10^{10} cm $Hz^{1/2}$ W^{-1} specific detectivity beyond 2 μm wavelength range operating at room temperature, which can already rival some commercial liquid nitrogen or thermoelectrically cooled photodetectors. To demonstrate the practical application of the QD phototransistor, we incorporated the device in a carbon monoxide gas sensing system and demonstrated reliable measurement of gas concentration. This work represents an important step forward in commercializing QD based infrared detection technologies.

Near-to-Mid infrared (IR) photodetection technologies have the potential to revolutionize the infrastructures of surveillance and manufacturing by enabling military or civil night vision[1,2], environmental gas monitoring[3] and chemical spectroscopic analysis[4]. However, current commercial IR photodetectors, particularly those with beyond 2000 nm spectral response, rely on expensive and size-limited epitaxial growth processes that are not compatible with silicon wafer technologies[5]. Furthermore, to achieve the desired signal-to-noise ratio, liquid nitrogen or two-stage thermoelectric cooling (TEC) is normally required to lower the operation temperature of

the photodetectors. This makes it impossible to achieve compact or miniaturized IR photodetection systems for applications such as sensor network and portable imagers and spectrometers. Given such limitations, a new generation of low-cost, room temperature-operated and sensitive IR photodetectors is highly desired.

Colloidal HgTe quantum dots (QDs), with a spectral response spanning almost the entire Near-to-Mid IR range[6,7,8], are a promising material candidate for the new generation photodetectors. However, long-wavelength HgTe QD based photodetectors have so far exhibited a rather low room-temperature specific detectivity (< 10^9 Jones (or cm $Hz^{1/2}$ W^{-1} in SI units))[9], more than one order lower than the detectivity achieved by commercial epitaxial IR photodetectors at low temperatures. The performance limitation stems from two main reasons. The first one is related to synthetic difficulties in producing high-quality QDs. The widely-used hot-injection method combined with organic solvent growth can effectively extend the absorption edge of HgTe QDs to the long wavelength IR range[8,10], however, rapid growth at high temperatures can result in a large amount of surface recombination centers, which significantly reduces the photoluminescence quantum yield (PLQY)[11] of the QDs. On the other hand, room temperature aqueous methods have been shown to allow high PLQY, but they are in practice limited to QD diameters of typically less than 5 nm (i.e. with emission ≤ 1800 nm)[12] unless combined with a subsequent heating stage to promote QD enlargement by Ostwald ripening[13]. It should be noted however that Ostwald ripening, particularly for aqueous solvent based systems, when pushed beyond certain limits can also have limitations such as poor QD size control and low PLQY[14]. The second reason for the poor performance of HgTe QD photodetectors is their unoptimized device structures. Due to the narrow bandgap of HgTe QDs, it is difficult to find a matching material that can form a Type II heterojunction with the QD film; therefore, nearly all the QD

photodetectors operated beyond 2000 nm spectral range are based on a photoconductor structure[7,8,9] rather than photodiodes as it has little requirement on energy level alignment. Unfortunately, the photoconductor structure offers very limited control on the distribution and transport of charge carriers in the semiconductor layer. This limitation could potentially be addressed by adding a "gating bias" through a field-effect transistor (FET) structure. FET structures have previously been used to characterize doping polarity and charge carrier mobility of HgTe QD[9] and HgSe QD[15] films, but it remains unclear whether they could outperform photoconductor structures by enabling tunability in the noise and gain of a photodetector.

In this study, we overcome the performance bottleneck of HgTe QD photodetectors through synergistic efforts between synthetic chemistry and device engineering. Firstly, we developed a fully automated aprotic solvent, gas-injection synthesis method that allows scalable fabrication of large sized HgTe QDs with high quality, exhibiting a record high PLQY for HgTe QDs of 17% at 2080 nm. Secondly, through layer-by-layer spray-coating of the QD layer we realized a HgTe QD based phototransistor with a pronounced gate effect at room temperature. This enabled us to perform a comprehensive parametric analysis on the photodetection performance in different transistor operation regimes, i.e. accumulation *vs.* depletion, based on which, we successfully realised the device to reach > 2×10^{10} Jones specific detectivity beyond 2000 nm wavelength range at room temperature, which can already rival the performance of liquid nitrogen or TEC cooled commercial MIR detectors[5]. The temperature dependent photocurrent and mobility analysis further reveal that the photosensing ability of our phototransistor can be maximized to close to 10^{11} Jones at 260 K, an operation temperature that is achievable by integrating the detector with a small-sized low-current driving TEC unit. To demonstrate the practical application of the QD phototransistor, we incorporated the device in a carbon monoxide

gas sensing system, where the device exhibited a reliable response to gas concentration fluctuations.

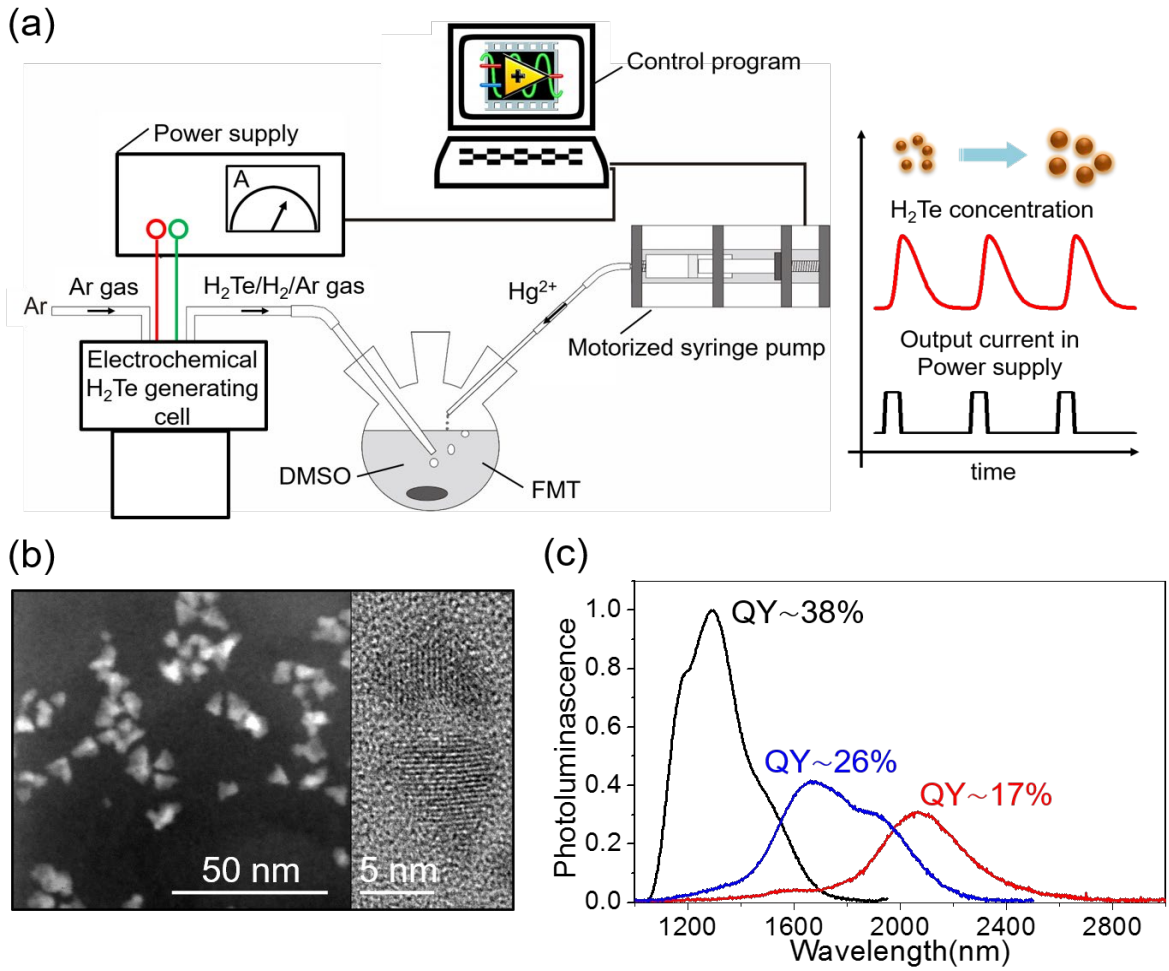

Figure 1. (a) The schematic setup of HgTe QD aprotic solvent, gas-injection synthesis with LabView automatic control panel. (b) Scanning-TEM image and typical TEM image of HgTe QDs (cast from toluene/dodecanethiol ligand solution with PL peak at about 2200 nm). (c) The typical PL spectra of HgTe QDs with the solution PL QY indicated.

The aprotic solvent, gas-injection synthesis (Fig. 1(a)) of HgTe QDs is a modified version of the aqueous synthetic approach where $Hg(ClO_4)_2$ reacts with H_2Te gas in the presence of 1-thioglycerol (TG) as a stabilizing ligand[12,16,17]. In the aqueous process, aggregation of HgTe QDs starts to prevail when the particle size increases to around 4 nm[18], hindering further growth of the QDs. In our approach, we introduced two modifications to avoid the aggregation process. Firstly,

we designed a fully automated precursor supply system, which enables us to inject repeated iterations of Hg^{2+} salt solution and H_2Te gas (electrochemically generated) at a coulombically controlled rate during the prolonged QD growth process. In this manner, by only introducing small amounts of these precursors in each iteration (followed by typically 10-20 min waiting time), we minimize the tendency of QD aggregation and obtain larger sized QDs without recourse to heating and ripening. Secondly, we choose dimethyl sulfoxide (DMSO) to replace water as the reaction solvent and paired it with 2-furanmethanethiol (FMT) as the stabilizing ligand[19,20]. FMT is a relatively short ligand and appears to have a moderate binding affinity for cations both in solution and at the surface of growing QDs. This strikes a reasonable balance between QD stabilization and solvation in DMSO, allowing continued growth of the QDs. DMSO as a solvent can support less hydrogen bonding than water, being only able to accept hydrogen bonds from acidic hydrogens on the ligand functional groups. This reduces the scope for supramolecular bond formation near the surface of the growing QDs, which may help to maintain good access of precursor ions to the surface and extend the size range for room temperature synthesis. Mercury (II) acetate is used as the Hg precursor because (i) the salt has a good solubility in DMSO, and (ii) a moderately hard base (acetate anion) paired with a relatively soft acid cation (Hg^{2+}) helps to favor QD formation[21,14], which possibly assists particularly at larger QD diameters.

Fig. 1(b) shows the transmission electron microscopy (TEM) images of the HgTe QDs, which are well-dispersed and exhibit triangle-shapes corresponding to tetrahedra or cube corners. We took three QD samples from different growth stages and examined their PLQY. As shown in Fig. 1(c), the QY is 38% for the small QDs emitting at 1200 nm, and it is still more than 17% for the large QDs emitting at 2100 nm. These PLQY values are much higher than those obtained from

hot-injection synthesis, which are typically in the range of 1% – 10%[11]. It is worth mentioning that the previous reported aqueous gas-injection / heating ripening combined process also yields a high QY of about 40% for the 1100 nm-emitting QDs; however, when the QDs are grown to emit at 2300 nm their QY dropped to below 11%[13]. Note that wavelength-dependent decrease of PLQY occurs naturally for IR QDs. According to Fermi's golden rule, the radiative recombination rate drops almost linearly with reduced emission frequency (i.e., increased emission wavelength), suggesting that the non-radiative recombination will become more dominant for large QDs [22]. Nevertheless, the QY of ~ 17% is the highest among the reported values for HgTe colloidal QDs that emit beyond 2000 nm.

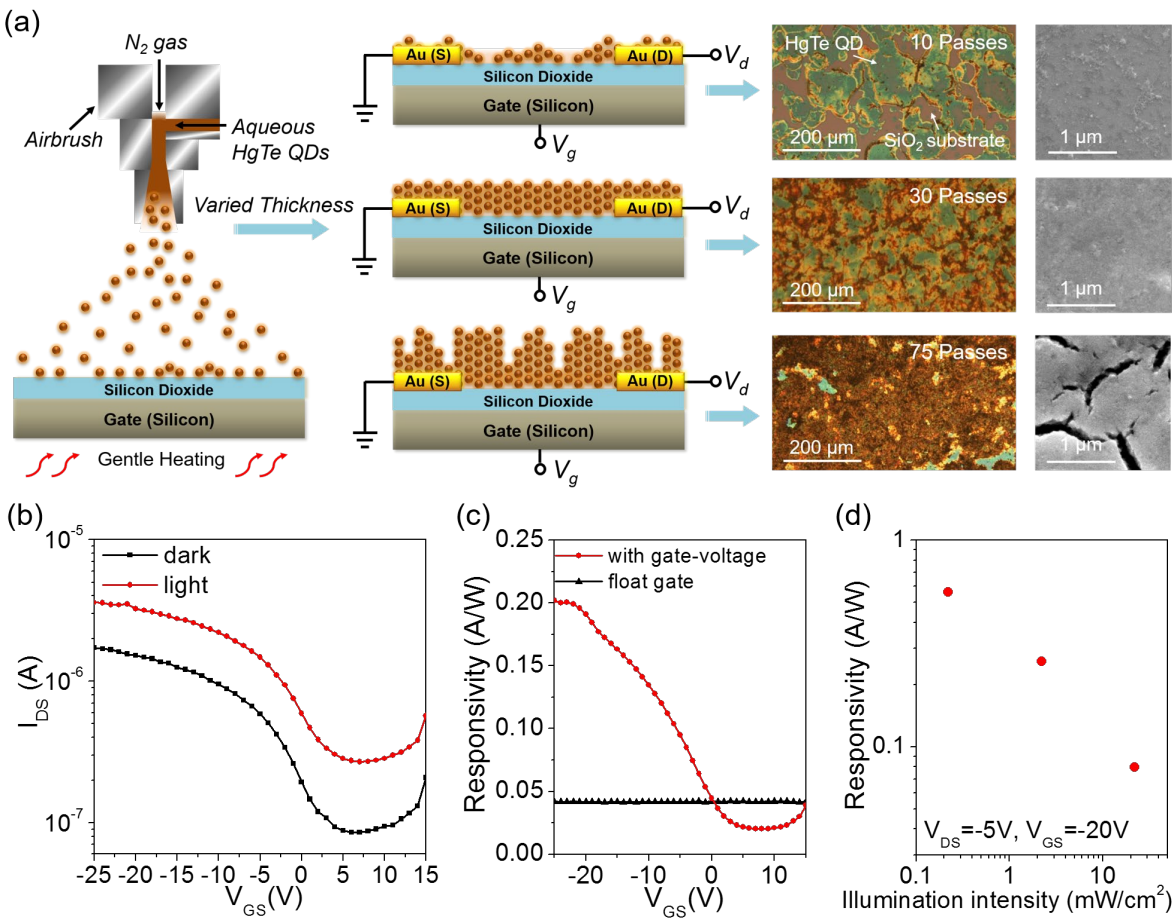

Figure 2. (a) Schematic of the spray-coating setup and the aqueous HgTe QD based phototransistor device structures with a range of QD film thicknesses deposited by a series of spray passes. The corresponding optical microscopy and SEM images of the QDs films are shown on the right. (b) Typical transfer characteristics of the aqueous HgTe QD based phototransistor (30 spray passes) under dark and illumination conditions. (c) The gate-voltage dependent responsivity of the phototransistor with the comparison to floating-gate operation. (d) Light intensity dependent responsivity of the phototransistor operated in accumulation mode. Illumination level in (b) and (c): 1550 nm, 4.2 mW cm^{-2}. All data are measured at room temperature (298 K).

For device fabrication, the QDs are re-dispersed in an aqueous solution following a two-step ligand exchange process from FMT to TG (see Methods for the details of the process.) Fourier transform infrared spectroscopy (FTIR) confirms that the ligand exchange process occurs effectively (Fig. S1 in the Supplementary Information). Next, a bottom-contact/bottom-gate transistor (Fig. 2 (a)) is fabricated using a heavily doped silicon substrate as the gate and its

oxide surface layer (~300 nm thick SiO_2) as the gate dielectric. The source and drain contacts are photolithographically patterned gold electrodes. To form the photoactive layer, the aqueous HgTe QD solution is spray-deposited onto the substrate with multiple passes in an ambient environment. The droplet size and spray speed are adjusted such that in each spray pass the QD droplets are sparsely distributed and instantly dried on the substrate surface. The QD film thickness and morphology evolve with the number of spray pass, as shown in the optical microscopy and scanning electron microscopy (SEM) images in Fig. 2(a). In the initial spray passes, the QD droplets gradually connected with each other but did not yet fully cover the substrate. From the 10^{th} to 30^{th} passes, the QD film started to form a full coverage layer while its thickness continued to grow. When the pass number further increased to 45 and above, the roughness of the film rapidly increased, accompanied with the emergence of cracks and aggregated particles in the films (Fig. 2(a) and Fig. S2(b)-(f) in the Supplementary Information). The morphology change is likely related to re-dissolution of the QDs deposited in previous passes: As the film becomes thicker, the re-dissolution sites accumulate. As a result, the film starts to behave like a sponge to absorb solvent from sprayed droplets but the thickened film releases the solvent far more slowly than the initial thinner layers, and the final drying process would therefore leave behind a cracked film.

Subject to the film morphology limitations the optimal number of spray passes can be determined based on the electrical response of the QD transistors, as shown in Fig. S2(a) in the Supplementary Information. It can be seen that the gate effect firstly increases from 10 to 30 spray passes and then decreases after 45 passes, which correlates well with the morphology variation. Since the phototransistor with a 30-pass sprayed QD film exhibits the highest transconductance and on/off ratio, we selected this device configuration for further parametric

analysis of photodetection performance. The QD film in this condition typically has a thickness around 80 nm.

The typical dark and light transfer characteristics of the optimized transistor are shown in Fig. 2(b). The device exhibits a predominant p-type behavior, similar to those made with near-IR aqueous HgTe QDs[23]. The suppression of the electron transport may be related to the surface non-stoichiometry[24] and/or the OH^- groups from the negatively charged TG ligands[25] and the SiO_2 surface. At room-temperature (RT), the on/off ratio of the transistor exceeds 20, indicating a significant gate effect in tuning the carrier density in the active layer. Such high RT on/off ratio was not achieved previously in organic-phase drop-cast HgTe QD transistors[9], and it can be attributed to the lower doping density enabled by the QD synthesis method used here and the suppression of n-type transport, which helps to reduce the recombination current.

We now turn to evaluate the photodetection performance of the QD transistor. The commonly used figure-of-merit of a photodetector is specific detectivity or noise-equivalent power (NEP), both of which are determined by the responsivity and noise current of the photodetector. The RT gate-voltage dependent responsivity of the QD transistor is shown in Fig. 2(c). As compared to the floating-gate operation (i.e., photoconductor mode), biasing the gate at -25 V (accumulation mode) can raise the responsivity by more than 4 times; while biasing the gate to +6 V (depletion mode) results in a responsivity drop of 50%. Such responsivity variation is likely associated with a trap-filling effect. For instance, in accumulation mode the gate-induced holes help to fill up the hole trap states; consequently, the photogenerated holes can transport in the accumulation layer with a higher mobility, resulting in a shorter transit time for holes in the channel. Our previous study[23] suggests that in the QD photodetectors the responsivity is proportional to the photoconductive gain, G, and that $G=\tau_c/\tau_t$ where τ_c is the trap lifetime; τ_t is the transit time of the

transport carrier. Hence, changing the transit time of the transport carriers (in this case, the holes) will result in variation of the responsivity.

The light intensity-dependence of responsivity in the accumulation mode is shown in Fig. 2(d). Under 0.22 mW cm^{-2} illumination, the responsivity reaches 0.56 A W^{-1}, which is comparable to the typical responsivity of commercial germanium photodetectors at 1550 nm. The responsivity of the QD device reduces at high light intensities, suggesting a loss of photoconductive gain. This is due to a transition from trap-assisted charge recombination to band-to-band charge recombination (also referred as bimolecular recombination) when the amount of photogenerated carriers are increased significantly. As shown in Fig. 3(a), the power law dependence of the photocurrent (I_{ph}) on the light intensity (I), i.e., $I_{ph} \propto I^{\alpha}$, can be fitted with α~0.56 in the accumulation mode and α~0.44 in the depletion mode. Both α values are close to 0.5, corresponding well to a bimolecular recombination dominated process[26] at high light intensities. The transient photocurrent decays (Fig. 3(b)) also suggest that bimolecular recombination dominates at the initial decay stage where charge carrier density is high, while that at the later stage the slower trap-assisted recombination process becomes dominant since the charge carrier density becomes low. The effective decay time constants τ_{eff} are measured to be about 12.6 μs and 10.2 μs in the accumulation and depletion modes respectively. Accordingly, the 3dB bandwidth f_{3dB} of the QD phototransistors is estimated to be on the order of ~10 kHz based on $f_{3dB}=1/(2\pi\tau_{eff})$ [23].

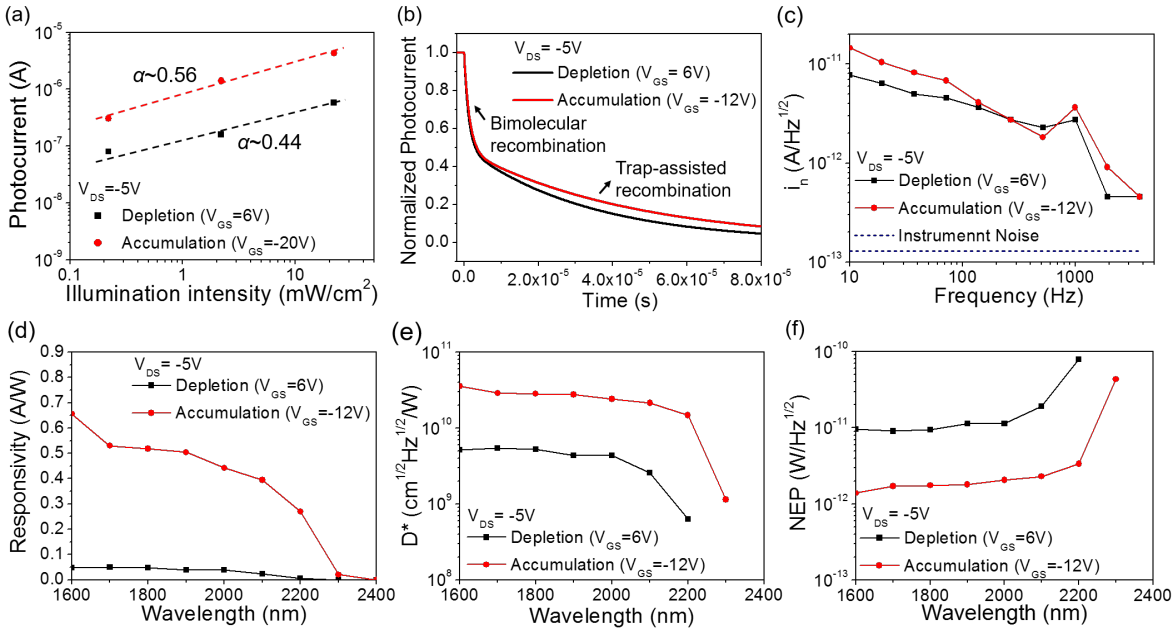

Figure 3. Light intensity dependent photocurrent and log-log fit (a), temporal response (b), current noise spectral density (c) and the wavelength dependent responsivity (d), specific detectivity (e) and noise-equivalent power (f) spectra of the HgTe QD based phototransistor (30 spray passes) operated in depletion mode and accumulation mode respectively. All data were measured at RT (298 K).

Noise current is another critical parameter that determines detectivity. It can be seen from Fig. 3(c) that both depletion and accumulation modes exhibit low 1/f noise current, suggesting that the noise characteristics are dominated by the nanocrystalline nature of the QD films[27,28]. The depletion mode exhibits lower noise current due to its lower dark current level. It is important to investigate the trade-off between the responsivity R and noise spectral density I_n through gate-voltage tuning, in order to achieve the optimized detectivity given by $D^* = R\sqrt{Area} / I_n$. Therefore, the device performances of the optimal phototransistor in both modes were characterized and compared (see Fig. S4 in Supplementary Information for noise measurement setup and the detailed discussion).

The wavelength dependent responsivity spectra of the optimal phototransistor in accumulation mode and depletion mode are compared in Fig. 3(d). More than 0.4 A W^{-1} responsivity is

achieved with the accumulation operation just beyond 2000 nm spectral range. The responsivity in accumulation mode is ten times larger than that in depletion mode over the whole spectrum. On the other hand, as suggested in Fig. 3(c), the noise level in the accumulation mode is only slightly higher than that in the depletion mode. As a result, higher detectivity should be obtained in the accumulation mode. We calculated the wavelength dependent detectivity (D^*) and noise-equivalent power (NEP) spectra of the QD based phototransistor using the noise spectral density at 2 kHz. As shown in Fig. 3(e), more than 2×10^{10} Jones specific detectivity and lower than 3×10^{-12} W $Hz^{-1/2}$ NEP were obtained with accumulation mode in the beyond-2000 nm spectral range.

It is worth emphasizing that all the above characterizations were conducted at RT. To the best of our knowledge, this is the first colloidal QD based photodetector that exhibits $>10^{10}$ Jones RT specific detectivity in the beyond-2000 nm wavelength range. This value can be further increased with higher drain- and gate-voltage operation or with the use of smaller channel length and high-*k* gate dielectrics. The spectral range can be extended to the mid IR range (e.g., 3000 – 5000 nm) with modified synthesis conditions. The excellent room-temperature photoresponse would make the technology highly competitive as typical commercial epitaxially-grown IR photodetectors rely on cooling (e.g., InSb detectors typically operate at 77 K with liquid nitrogen cooling[29], HgCdTe detector operate at 230 K with two-stage TEC cooling[30]) to provide 1×10^9 – 8×10^{11} Jones detectivity.

To explore the optimal operation temperature of the photodetector, we also characterized the temperature-dependent transport properties of the QD transistor. Fig. 4(a) shows the dark transfer characteristics measured from 300 K to 140 K, based on which the hole mobility as a function of temperature is calculated and plotted in Fig. 4(b). The mobility first rises with temperature and

then reaches a plateau at 260 K to 220 K. The increase of mobility may result from a reduction of the barrier width for charge tunneling between the QDs, which is caused by the thermal contraction of the ligands, as reported in other QD systems[31,32]. Below 220 K, the mobility decreases as temperature drops, manifesting a thermally-activated charge hopping process with an activation energy E_a of 25.6 meV. We also note that the n-type behavior starts to appear at low-temperatures. This is because the gating-effect in introducing electrons becomes more effective as the amount of thermally generated charge carriers is reduced.

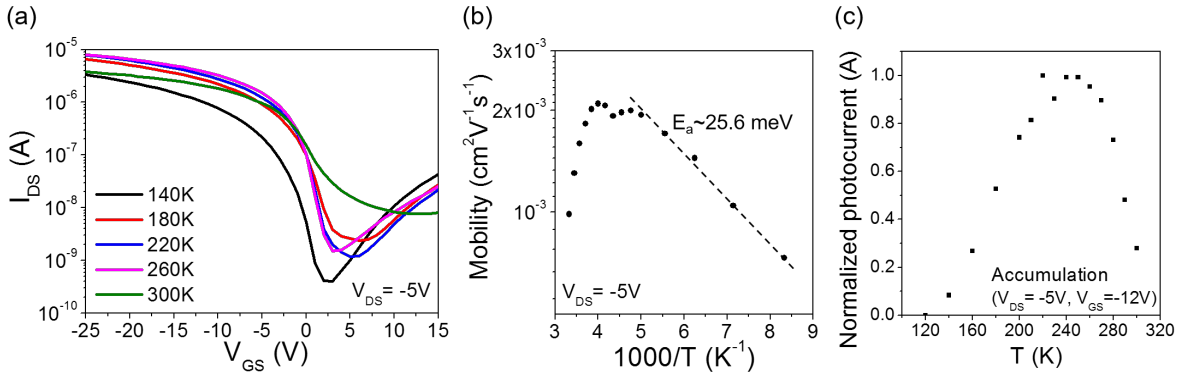

Figure 4. (a) Dark transfer characteristics of the HgTe QD phototransistor in a semi-logarithmic scale. (b) Temperature dependent hole mobility and the fitting (dashed line) for the low temperature activation energy. (c) Temperature dependent normalized photocurrent of the phototransistor operated in accumulation mode (1550 nm, 2.2 mW/cm^2 illumination).

With the increased hole mobility and electron trapping time, the photoconductive gain of the transistor is expected to reach its maximum close to 260 K. As shown in Fig. 4(c), the photocurrent at 260 K is three times larger than the room temperature photocurrent. As the 1/f noise should decrease at low temperatures[28], a specific detectivity close to 10^{11} Jones could be obtained. It is worth mentioning that this temperature is only 40 K away from the RT and can be achieved with a small and compact low-current TEC temperature control unit[33].

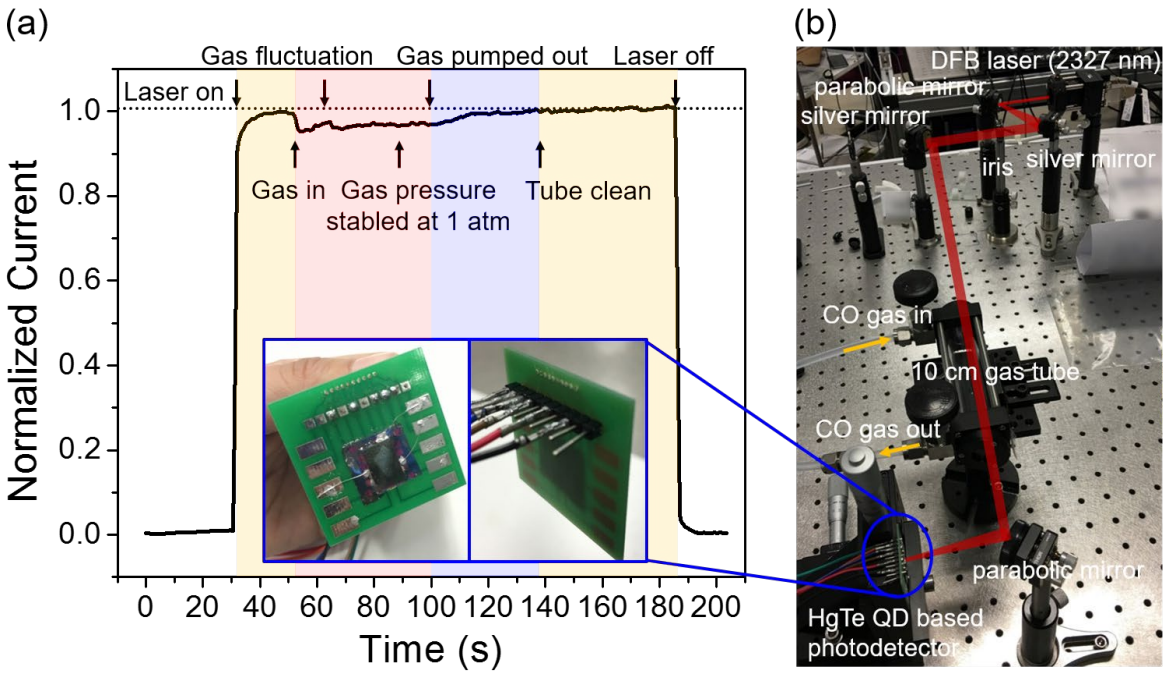

Figure 5. (a) Normalized room-temperature photocurrent response of the HgTe QD based phototransistor during the CO gas sensing measurement; (b) photograph of the experimental setup of the gas sensing system. Inset of (a): Photos of the packaged phototransistor.

Finally, to demonstrate the potential application of the HgTe QD based phototransistor in gas sensing applications, we integrated it into a single-pass carbon monoxide (CO) gas sensing system as the photodetection unit. A photograph of the system is shown in Fig. 5(b), where a laser light with its wavelength tuned to the R(10) line of CO (~ 2327 nm) is directed through a 10 cm long gas cell and then focused onto the phototransistor mounted on a printed circuit board (inset of Fig. 5(a)). During the measurement, the gas cell is first ventilated with a nitrogen/CO gas mixture (0.9% CO concentration) at a controlled pressure (1 bar) and then evacuated into vacuum. The corresponding current response of the phototransistor is recorded as a function of time. The normalized current response during the whole measurement process is shown in Fig. 5(a). The phototransistor has a sharp response to the illumination at the moment being turned on/off. When CO is introduced into the cell, the photocurrent drops immediately due to the light

absorption by CO. We note that the photocurrent is sensitive to the concentration variation of CO: both the gas fluctuation during ventilation and the pump-out process of CO can be resolved. Based on the photocurrent drop at the stabilized gas pressure, the absorption coefficient of CO at 2327 nm is measured to be 3.5×10^{-3} cm^{-1}, which is close to the theoretical value of 3.6×10^{-3} cm^{-1} calculated from the HITRAN database[34] at room temperature, atmospheric pressure and with a CO gas concentration of 0.9%[35].

In summary, we have demonstrated a HgTe QD based photodetector that exhibits above 2×10^{10} Jones specific detectivity beyond 2 μm wavelength range at room temperature operation. Several key elements to enable such high performance are discussed. Firstly, the fully automated aprotic solvent, gas-injection synthesis allows well-controlled fabrication of high quality HgTe QDs. Secondly, the layer-by-layer spray-coating process enables thickness optimization of the QD layer to realize a gating effect in the transistor structure at room temperature. Finally, bias-dependent photodetection parameters, including responsivity, noise and bandwidth, are analyzed to reveal the optimal operation window for high detectivity. The successful implementation of the QD photodetector in a harmful gas sensing system demonstrates its promising potential in enabling portable sensing devices or sensor networks. Our findings shed light on the fundamental elements that enable commercialization of QD based infrared detection technologies.

METHODS

HgTe QD synthesis

The electrochemical cell generated a mixture of H_2 and H_2Te via electrolysis of phosphoric acid solution using a Te anode and Pt cathode. The mixture of gases was passed over into the reaction flask in a steady stream of argon gas. The electrolysis current was supplied by a power supply

unit operating in current regulated mode. Additional Hg^{2+} salt solution in DMSO could be added via a syringe pump. The power supply unit and the syringe pump were controlled by a computer running a LabView program. The reaction was carried out under argon in a 500ml 3 necked reaction flask with a magnetic stirrer.

Ligand exchange and precipitation process.

The purpose of each of the three different solvent/ ligand stages described below are: initial room temperature growth in DMSO with FMT ligand to obtain improved QD surface quality; transfer to tetrachloroethylene (TCE) with dodecanethiol (DDT) ligand for spectroscopy and characterization and to move out of DMSO which has too high a boiling point for spin coating or spray coating film formation; transfer to water and 1-thioglycerol (1-TG) where the ligand length is short and improves film conductivity (closer QD packing) and spray coating is possible.

QDs prepared in DMSO with FMT ligands were transferred into TCE solution and the FMT replaced with (DDT) ligands. DMSO is strongly absorbing in the IR and FMT is not compatible with the TCE solvent. After ligand exchange the solution was purified several times to reduce the DDT concentration to the minimum level required to stabilize the QDs in TCE. For the spray fabrication of devices, the QDs have been further transferred from TCE/DDT solution into water with 1-TG replacing the DDT ligands. The QDs were initially transferred into a 5:1 tetrahydrofuran (THF) / n-methyl pyrollidone solution to facilitate the displacement of the DDT ligand in favour of the 1-TG when transferring the QDs into aqueous solution. After the QDs have partitioned into the aqueous phase, any organically soluble content was removed by washing the water-based solution with toluene. Excess 1-TG was removed by precipitating the aqueous phase with acetonitrile followed by centrifugation. The dried precipitate was then re-dissolved in water and used for spray coating deposition.

Device fabrication

The silicon wafers with pre-patterned gold interdigitated electrodes (15 periods, 1 mm long and 5 μm spacing) were prepared photolithographically, using metal thermal deposition and a lift-off process. After 100 seconds oxygen plasma treatment, the samples were heated gently on a 55 ˚C hotplate for spray deposition in an ambient environment. The airbrush (Tamiya SparMax SX3.0D) with a nozzle size of 0.3 mm was fixed 11.4 cm above the hotplate. The flow rate of the HgTe QD solution was controlled by the gas pressure (0.3~0.5 bar). The film samples were washed-out with a 1:2 methanol: acetonitrile solution to remove residual Na^+ ions and then encapsulated under glass slides under nitrogen atmosphere in a glove box.

Characterization

The SEM imaging was carried out on an FEI Quanta 400 FEG microscope. The current-voltage characteristics were measured with a Keithley 2612 Source Meter illuminated by a Newport LQD1550E 5 mW 1550 nm laser. The light intensity dependent properties were calibrated with the same setup with a NIR absorptive filter. The wavelength dependent responsivity was measured with a Keithley 2612 Source Meter under monochromatic illumination generated by passing the light beam from a 250W quartz tungsten halogen (QTH) lamp into a Newport 74125 Oriel Cornerstone 260 1/4 m monochromator. The optical power density was measured to be about 1 mW/cm^2 at λ=800 nm. The light passed through a 1500 nm long pass filter and was focused by two CaF_2 lenses onto the samples. A Hamamatsu P5968-200 InSb photovoltaic detector was used to calibrate the optical power density. The reference InSb photodetector was operated at 80 K with liquid nitrogen cooling.

For transient photocurrent measurement, all devices were biased with a Keithley 2612 Source Meter and illuminated by a function generator (Agilent 33210A) modulated Newport LQD1550E

laser with 11 Hz repetition frequency. The resulting photocurrent was amplified by a Femto DHPCA-100 High Speed Current Amplifier and recorded with a Tektronix TDS 3014C Oscilloscope.

For noise current spectral density measurement, devices were sealed in a metal shielding box with battery biased source-drain and gate-drain voltages. A lock-in amplifier (Stanford Research 830) was connected in series to the test device to measure the noise current at different frequencies with measurement unit A $Hz^{-1/2}$. The impedance of the lock-in amplifier was 1 kΩ, which was much smaller than the source-drain resistance of the device (larger than 1 MΩ even where a gate voltage was applied). It should be noted that the current input to the lock-in amplifier should be no larger than 10 μA and the latter's internal noise current limit was 130 fA $Hz^{-1/2}$.

Acknowledgements

Author contributions

Additional information

References

1. Hansen, M. P. & Malchow, D. S. Overview of SWIR detectors, cameras, and applications. *Proc. of SPIE* **6939,** 69390I-1 (2008).
2. Schreiner, K. Night vision: infrared takes to the road. *IEEE Comput. Graph. Appl.* **19,** 6–10 (1999).

3. Stepanov, E. V., Kouznetsov, A. I., Zyrianov, P. V., Plotnichenko, V. G. & Selivanov, Yu. G. Multicomponent fiber-optical gas sensor based on MIR tunable diode lasers. *Infrared Phys. Technol.* **37,** 149–153 (1996).

4. Bacon, C. P., Mattley, Y. & DeFrece, R. Miniature spectroscopic instrumentation: Applications to biology and chemistry. *Rev. Sci. Instrum.* **75,** 1–16 (2004).

5. Rogalski, A. Recent progress in infrared detector technologies. *Infrared Phys. Technol.* **54,** 136–154 (2011).

6. Böberl, M., Kovalenko, M. V., Gamerith, S., List, E. J. W. & Heiss, W. Inkjet-printed nanocrystal photodetectors operating up to 3 μm wavelengths. *Adv. Mater.* **19,** 3574–3578 (2007).

7. Keuleyan, S., Lhuillier, E., Brajuskovic, V. & Guyot-Sionnest, P. Mid-infrared HgTe colloidal quantum dot photodetectors. *Nat. Photonics* **5,** 489–493 (2011).

8. Keuleyan, S. E., Guyot-Sionnest, P., Delerue, C. & Allan, G. Mercury telluride colloidal quantum dots: electronic structure, size-dependent spectra, and photocurrent detection up to 12 μm. *ACS Nano* **8**, 8675-8682 (2014).

9. Lhuillier, E., Keuleyan, S., Zolotavin, P. & Guyot-Sionnest, P. Mid-infrared HgTe/As_2S_3 field effect transistors and photodetectors. *Adv. Mater.* **25,** 137–141 (2013).

10. Keuleyan, S., Lhuillier, E. & Guyot-Sionnest, P. Synthesis of Colloidal HgTe Quantum Dots for Narrow Mid-IR Emission and Detection. *J. Am. Chem. Soc.* **133,** 16422–16424 (2011).

11. Keuleyan, S., Kohler, J. & Guyot-Sionnest, P. Photoluminescence of mid-infrared HgTe colloidal quantum dots. *J. Phys. Chem. C* **118,** 2749–2753 (2014).

12. Kershaw, S. V., Susha, A. S. & Rogach, A. L. Narrow bandgap colloidal metal chalcogenide quantum dots: synthetic methods, heterostructures, assemblies, electronic and infrared optical properties. *Chem. Soc. Rev.* **42,** 3033–3087 (2013).

13. Kovalenko, M. V., Kaufmann, E., Pachinger, D., Roither, J., Huber, M., Stangl, J., Hesser, G., Schäffler, F. & Heiss, W. Colloidal HgTe nanocrystals with widely tunable narrow band gap energies: from telecommunications to molecular vibrations. *J. Am. Chem. Soc.* **128**, 3516–3517 (2006).

14. Jing, L., Kershaw, S. V., Li, Y., Huang, X., Li, Y., Rogach, A. L. & Gao, M. Aqueous Based Semiconductor Nanocrystals. *Chem. Rev.* **116,** 10623-10730 (2016).

15. Lhuillier, E., Scarafagio, M., Hease, P., Nadal, B., Aubin, H., Xu, X. Z., Lequeux, N., Patriarche, G., Ithurris, S. & Dubertret, B. Infrared photodetection based on colloidal quantum-dot films with high mobility and optical absorption up to THz. *Nano Lett.* **16,** 1282–1286 (2016).

16. Rogach, A., Kershaw, S., Burt, M., Harrison, M., Kornowski, A., Eychmüller, A. & Weller, H. Colloidally prepared HgTe nanocrystals with strong room-temperature infrared luminescence. *Adv. Mater.* **11,** 552–555 (1999).

17. Harrison, M. T., Kershaw, S. V., Burt, M. G., Eychmüller, A., Weller, H. & Rogach, A. L. Wet chemical synthesis and spectroscopic study of CdHgTe nanocrystals with strong near-infrared luminescence. *Mater. Sci. Eng.* ***B*69–70,** 355–360 (2000).

18. Kershaw, S. V. & Rogach, A. L. Infrared emitting HgTe quantum dots and their waveguide and optoelectronic devices. *Z. Phys. Chem.* **229(1-2)**, 23–64 (2015).

19. Nijssen, L. M., Visscher, C. A., Maarse, H., Willemsens, L. C. & Boelens, M. H. *Volatile compounds in food: qualitative and quantitative data, 7th ed*., TNO Nutrition and Food Research Institute: Zeist, The Netherlands, pp 72.1-72.23 (1996)

20. Blank, I., Sen, A. & Grosch, W. Aroma impact compounds of arabica and robusta coffee. Qualitative and quantitative investigations. *ASIC. 14e Colloque. San Francisco,* 117–129 (1991).

21. Izquierdo, E., Robin, A., Keuleyan, S., Lequeux, N., Lhuillier, E. & Ithurria S. Strongly confined HgTe 2D nanoplatelets as narrow near infrared emitters. *J. Am. Chem. Soc.* **138**, 10496−10601 (2016).

22. Wen, Q., Kershaw, S. V., Kalytchuk, S., Zhovtiuk, O., Rechmeier, C., Vasilevskiy, M. I. & Rogach, A. L. Impact of D_2O/H_2O solvent exchange on the emission of HgTe and CdTe quantum dots: polaron and energy transfer effects. *ACS Nano* **10**, 4301−4311 (2016).

23. Chen, M., Yu, H., Kershaw, S. V., Xu, H., Gupta, S., Hetsch, F., Rogach, A. L. & Zhao, N. Fast, air-stable infrared photodetectors based on spray-deposited aqueous HgTe quantum dots. *Adv. Funct. Mater.* **24,** 53–59 (2014).

24. Oh, S. J., Berry, N. E., Choi, J.-H., Gaulding, E. A., Lin, H., Paik, T., Diroll, B. T., Muramoto, S., Murray, C. B. & Kagan, C. R. Designing high-performance PbS and PbSe nanocrystal electronic devices through stepwise, post-synthesis, colloidal atomic layer deposition. *Nano Lett.* **14,** 1559–1566 (2014).

25. Lee, S., Koo, B., Shin, J., Lee, E., Park, H. & Kim, H. Effects of hydroxyl groups in polymeric dielectrics on organic transistor performance. *Appl. Phys. Lett.* **88,** 162109 (2006).

26. R. H. Bube, *Photoconductivity of Solids*, John Wiley and Sons, Inc., New York, Vol. 3, (1960).

27. Lhuillier, E., Keuleyan, S., Rekemeyer, P. & Guyot-Sionnest, P. Thermal properties of mid-infrared colloidal quantum dot detectors. *J. Appl. Phys.* **110,** 033110 (2011).

28. Liu, H., Lhuillier, E. & Guyot-Sionnest, P. 1/f noise in semiconductor and metal nanocrystal solids. *J. Appl. Phys.* **115,** 154309 (2014).

29. InSb photovoltaic detectors | Hamamatsu Photonics. Retrieved December 30, 2016, from https://www.hamamatsu.com/eu/en/product/category/3100/4007/4140/index.html

30. VIGO SYSTEM S.A. - PVI-2TE. Retrieved December 30, 2016, from http://www.vigo.com.pl/products/infrared-detectors/Photovoltaic-Detectors/pvi-2te-series

31. Ju, T., Graham, R. L., Zhai, G., Rodriguez, Y. W., Breeze, A. J., Yang, L., Alers, G. B. & Carter, S. A. High efficiency mesoporous titanium oxide PbS quantum dot solar cells at low temperature. *Appl. Phys. Lett.* **97,** 043106 (2010).

32. Loef, R., Houtepen, A. J., Talgorn, E., Schoonman, J. & Goossens, A. Temperature dependence of electron transport in CdSe quantum dot Films. *J. Phys. Chem. C* **113,** 15992–15996 (2009).

33. DiSalvo, F. J. Thermoelectric cooling and power generation. *Science* **285,** 703-706(1999).

34. Rothman, L. S. *et al.* The HITRAN 2008 molecular spectroscopic database. *J. Quant. Spectrosc. Radiat. Transf.* **110,** 533–572 (2009).

35. Li, Z., Wang, Z., Wang, C. & Ren, W. Optical fiber tip-based quartz-enhanced photoacoustic sensor for trace gas detection. *Appl. Phys. B* **122,** 147 (2016).